Available online at www.sciencedirect.com

ScienceDirect

Advances in Space Research xxx (xxxx) xxx

ADVANCES IN SPACE RESEARCH (a COSPAR publication)

www.elsevier.com/locate/asr

Performance of the IVS R1 and R4 sessions

Cynthia C. Thomas [a,*], Daniel S. MacMillan [a], Karine Le Bail [b]

[a] NVI Inc/NASA Goddard Space Flight Center, 7257 Hanover Parkway Suite D, Greenbelt, MD 20770, United States
[b] Onsala Space Observatory, Chalmers University of Technology, Observatorievagen 90, SE-439 92 Onsala, Sweden

Received 6 November 2022; received in revised form 10 July 2023; accepted 12 July 2023

Abstract

The International VLBI Service for Geodesy and Astrometry (IVS) has observed the weekly IVS-R1 (R1) and IVS-R4 (R4) series of sessions since 2002. These regular series are generally stable in the sense that the networks were designed to be similar from week to week. The uniformity of these series has allowed researchers to conduct many scientific investigations. The IVS also observes with other networks that allow continued sampling of data from all VLBI stations, but the R1 and R4 observing sessions are a dominant part of overall VLBI observing accounting for 1841 sessions out of a total of 3129 24-hour sessions from 2002.0 to 2020.0 (where the last R1 and R4 in 2019 was on December 30 and December 26, respectively). In this paper, we investigate the evolution of these series in terms of their observing networks. We also discuss the construction of the R1 and R4 networks and the scheduling of these sessions. The performance of these networks in terms of the formal precision of polar motion have improved by factors of 2–3 over the period from 2002.0 to 2018.0. UT1 precision improved by a factor of about 1.2–1.5. The main reason for this improvement is the increased size of the networks. We also discuss the effect on this improvement arising from changes in the data rate and the number of observed sources. There is some degradation in performance after 2018 that is most likely due to a decline in the number of available network stations.

Keywords: IVS-R1; IVS-R4; EOP; VLBI

1. Introduction

Very long baseline interferometry (VLBI) is a geodetic technique that measures signals from extragalactic radio sources observed with networks of ground-based antennas. A VLBI session consists of the delays measured between baseline stations in the network over a typical 24-hour observing period. A single observed delay (observation) is a baseline observable equal to the time delay between the times when a signal is received at the two stations in the baseline. A scan is defined as the set of all observations of the same source at the same epoch observed by antennas in the network. Observations are made at both S-band and X-band so that the ionospheric contribution to the delay can be removed. Geodetic sessions have been observed since 1979. Since 2000, the observations from geodetic networks have been coordinated by the International VLBI Service for Geodesy and Astrometry (IVS) (Schlüter and Behrend, 2007; Nothnagel et al., 2017).

One of the primary IVS goals is to provide Earth Orientation Parameters (EOP) for the scientific community. This includes operational users like the US Naval Observatory (USNO) or the Jet Propulsion Laboratory (JPL) who generate EOP combination series for scientific use. For this reason, the IVS has been organizing the observation of the weekly 24-hour IVS-R1 (R1) and IVS-R4 (R4) sessions since January 2002 with the main objective of providing regular EOP estimates. The R4 sessions replaced the weekly National Earth Orientation Service (NEOS)

* Corresponding author.
E-mail addresses: cynthia.c.thomas@nasa.gov (C.C. Thomas), daniel.s.macmillan@nasa.gov (D.S. MacMillan), karine.lebail@chalmers.se (K. Le Bail).

https://doi.org/10.1016/j.asr.2023.07.020
0273-1177/© 2023 Published by Elsevier B.V. on behalf of COSPAR.

network (two-week rapid turnaround program) that was observed from 1994 to 2001 (Schlüter and Vandenberg, 2003). The R1s grew out of the Continuous Observations of the Rotation of the Earth (CORE) program that began in 1997 (Thomas & MacMillan, 2003). CORE-A experiment sessions were observed on the same days as NEOS experiments, which allowed comparison of EOP from simultaneous networks and the derivation of network biases and precision (Ryan and Ma, 1998). MacMillan and Ma (2007) assessed different methods to model radio source instability by analyzing the EOP differences from these pairs of simultaneous NEOS and CORE-A experiments. CORE-B sessions were observed on days immediately following CORE-A sessions. The CORE-A, CORE-B, and NEOS experiments all employed six-station networks. In 2001, these were replaced by the CORE sessions. The concept of the CORE sessions was to eventually observe continuously every day of the week (Ryan and Ma, 1998).

Beginning in 2002, VLBI observed operationally each week with the R1 network mostly on Mondays and the R4 network mostly on Thursdays. The IVS planned to eventually observe in an operationally continuous mode. In 2002, only two days per week were possible for EOP sessions given station and media resources. Nevertheless, continuous observing is one of the key goals of the VLBI Global Observing System (VGOS) observations, which is the next-generation VLBI system currently being built (Niell et al., 2018). In contrast to the S/X band R1 and R4 sessions, VGOS sessions are observed in broadband mode in four bands from 2 to 14 GHz.

Many researchers have used the operational R1 and R4 series to conduct geodetic investigations, because the networks regularly observe every week and are generally stable. Some examples of these investigations are as follows. Malkin (2009) discussed the relationship between VLBI network properties and the quality of EOP. Böhm and Schuh (2004) evaluated the quality of the Vienna mapping functions with the R1 and R4 sessions. Since the VLBI antenna at Fairbanks (GILCREEK) in Alaska observed in the R1 experiments, the resulting position time series was used to investigate the Denali Earthquake (Titov and Tregoning, 2005; MacMillan and Cohen, 2004). Plank et al. (2015) investigated the performance of Southern Hemisphere observing stations using the R1 and R4 sessions. MacMillan (2017) compared the EOP precision of the CONT continuous observing campaigns with the EOP precision of the R1 and R4 experiments. Klopotek et al. (2018) used the R1 and R4 network schedules in 2014 to perform simulations to determine the position of a radio transmitter on the surface of the Moon with geodetic VLBI.

The objectives of this paper are to 1) describe how these sessions were developed and how they were scheduled and 2) examine the precision and accuracy of EOP estimates from R1 and R4 sessions observed from 2002 through 2020. The R1 and R4 sessions began in January 2002 with six-station networks (Thomas and MacMillan, 2003; Kingham and Carter, 2002). The network size increased over time to networks as large as 14 stations. There is a significant variation in observed EOP precision over different time periods within the 2002.0–2020.0 time span. The predominant cause of improved EOP precision is the increase in size and global distribution of the networks. Other factors that could explain the variability in observed EOP precision are network station variation, number of sources observed, data loss, and recording rate. All these factors are examined in our analysis of the performance of the R1 and R4 series.

In the next section, we begin with the history of the R1 and R4 networks. Section 2.1 describes how the characteristics of R1 and R4 data have changed. Section 2.2 discusses the evolution of the R1 and R4 networks in terms of their station compositions and the number of observations per session. Section 3.1 describes the annual process of constructing networks for all observing days for the following calendar year of observing. Section 3.2 provides details on the different scheduling parameters that have been used. Radio source selection is discussed in Section 3.3. Section 4 consists of an analysis of observed data in light of factors discussed in Sections 2 and 3. First, we consider the general trends of improvement of the formal EOP uncertainties in Section 4.1. The possible factors that contributed to the general improvement of EOP uncertainties are discussed in Section 4.2. Section 4.3 presents the results of comparisons of polar motion estimates from R1 and R4 networks with respect to Global Navigation Satellite Systems (GNSS) estimates. These comparisons provide a measure of observed VLBI polar motion precision and accuracy. A summary of the conclusions of our investigation is presented in Section 5.

2. History of the R1 and R4 networks

2.1. R1 and R4 data

Since 2002, the IVS has observed operationally each week with the R1 network on Mondays and the R4 network on Thursdays. Occasionally, the sessions may shift by a day due to holidays. It was planned to eventually observe operationally continuously; however, only two days per week were possible from the outset for EOP sessions given station and media resources. When the IVS program began in 2002, magnetic tapes were used for recording (in the Mark IV recording mode) for each session. The Mark IV system recorded up to a maximum total data rate of 1024 Mbps (expandable to 2048 Mbps) (Whitney, 2005).

In mid-2003, the IVS program started using the Mark 5 recording system and by the end of 2007 all stations were upgraded to Mark 5, which supports data rates up to 2048 Mbps. The Mark 5 recording mode uses a modern disk-based system, which 1) is easier to use and has a lower failure and problem rate, 2) enabled higher bandwidth

recordings to yield improvements in results through greater precision of the observables, 3) reduced costs associated with tape and recorders, which require significant technical staff resources to maintain and process (for more information, see Vandenberg and Whitney, 2003). Due to the efficiency of the Mark 5 correlator, the program then became dependent on station availability and media storage (Thomas and MacMillan, 2020).

For the IVS to meet the goal of 15-day latency (time between observation and the generation of a correlated database) to rapidly produce the data from the R1 and R4 sessions, some changes were required: availability and reliability of stations, automation for unattended observing, switching from tapes to disks, transferring data electronically, correlators giving higher priority to rapid sessions, and more IVS Analysis Centers with different software to increase product robustness (Schlüter and Vandenberg, 2003). The achieved availability and reliability of stations for the R1 and R4 sessions is shown in Section 2.2, which discusses how the networks evolved from six to up to 14 stations over the 2002.0 to 2020.0 period using a pool of 24 stations to build different networks. Automation for unattended observing was attained for Ishioka and the AuScope antennas (Hobart, Katherine, and Yarragadee). AuScope antennas were designed and created to be remotely controlled and monitored to lower operating costs as much as possible (Lovell et al., 2014). However, the unattended and remote features could only be achieved at a few stations. By the end of 2019, most stations could send their data via electronic transfer. The R1 and R4 sessions then were given high priority with the goal of processing and releasing the data for each session by the correlators within 15 calendar days of observation. The R1 sessions are being correlated by the Bonn Correlator in Germany and the R4 sessions are being processed by the Washington Correlator in Washington, DC, USA. For the most part the correlators have met this goal.

2.2. Network evolution

During the early years of the R4s, the number of Southern Hemisphere stations was limited. Fig. 1 indicates that TIGOCONC was the only far South station that was used consistently although HartRAO-26 m was used a few times. On the other hand, the R1s observed with HartRAO-26 m, TIGOCONC, and Hobart-26 m in the early years. In 2010–2011, Hobart-12 m, Yarragadee-12 m, and Katherine-12 m began consistently observing in the R1s and R4s. As more Southern stations were added to the R4 network, EOP precision improved. This includes the Warkworth station in New Zealand along with the full Australian AuScope network. HartRAO-15 m also began observing for the R1s and R4s in 2013–2014. Although AuScope will be switching to VGOS observing, HartRAO-15 m and Warkworth will still participate in R1 and R4 sessions until mixed-mode observations are operational and the other AuScope stations will be able to participate. Mixed-mode sessions include S/X only stations and VGOS stations that observe with a broadband receiver. In this case, the broadband receiver has sufficient bandwidth at S/X to allow the VGOS antenna to observe with S/X only stations as well as observing with other VGOS stations. We describe the changes to the R1 and R4 networks in detail from 2002 through 2020 in Appendix A.

Over the 2002–2020 period, the size of the networks generally increased from 4 to 6 stations to 8–14 stations as shown in Fig. 2. Although there were 24 stations available to participate in the R1 and R4 sessions during 2019, the actual maximum number of participating stations in a session was not larger than 14 stations due to station availability. Considering all observing stations, the station availability given in Table 1 for R1 and R4 sessions ranged from 5 to 52 days per station per year. This large variation in available station days resulted in several different networks for both the R1 and R4 sessions. Lambert and Gontier (2006) found that observing with a large number of stations is an advantage in estimating the TRF, but a changing network can degrade the estimation of a TRF. A large core network of stations observing in each session helps to alleviate this problem. This problem will continue to exist in the R1 and R4 sessions unless a specific set of core stations is scheduled to observe each session weekly; but this is unlikely given budgets and other station constraints. The prevalence of antennas, which are not dedicated to geodesy and which have competing usages of their antenna time, does not allow the S/X system to have large repetitive R1/R4 networks.

The maps in Fig. 2 and the corresponding Table 1 show how the R1 and R4 networks have evolved globally. One of the recurring issues for VLBI networks is the lack of antennas in the Southern Hemisphere compared to the Northern Hemisphere where the available land area is much greater. One can see from the maps that the global distribution of stations has improved specifically with the introduction of new southern stations, which provide more North-South baselines. In concert with these changes, we will see in Section 4 that the EOP performance of the networks improved mainly for polar motion.

As seen in Table 1, there were only two stations in the Southern Hemisphere observing in the R1 and the R4 sessions in 2002. This number increased significantly until 2016–2017. In 2002, the core station networks were composed of four stations (Gc, Wz, Wf, and Ma for R1 sessions and Ny, Wz, Ap, and Kk for R4 sessions), which are all in the Northern Hemisphere. By 2016, stations in the south (Ft, Ke, Ht, and Yg) were added to the core stations for both the R1 and R4 networks. Hb observed from 2010 to 2017.5 but the transition to VGOS equipment ended its participation in R1 and R4 sessions.

Figs. 1 and 2 and Table 1 show that the network size for both the R1 and R4 sessions increased. Depending on the network, the increased number of stations caused the number of observations to increase. The R1 first increased in

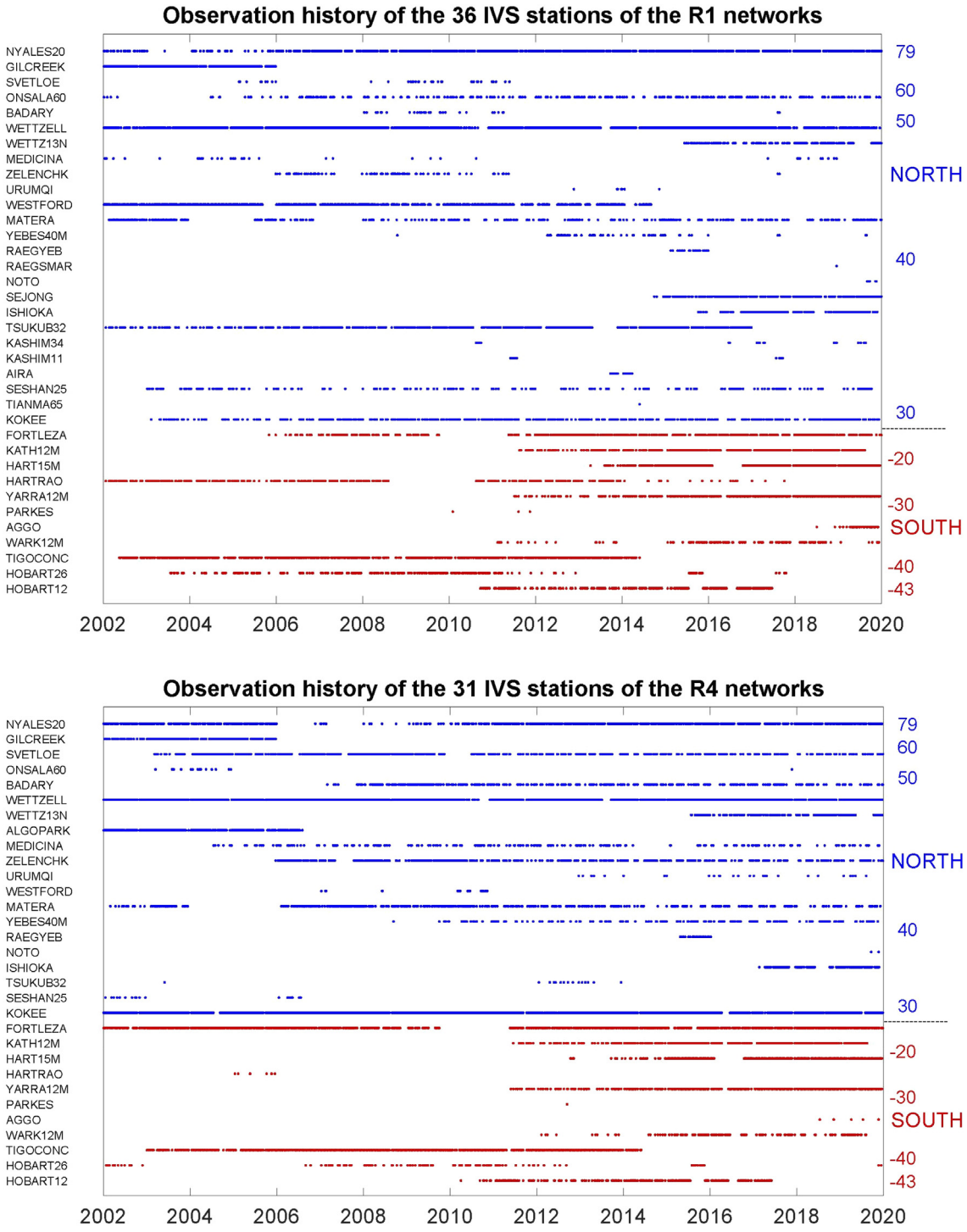

Fig. 1. R1 and R4 station observing histories for the period of 2002 through 2020.

network size in 2004 to 7 stations and to 8 stations in 2006. There was a more significant increase in 2011 to 9–10 stations and then to more than ten stations in 2014. The R4 sessions first increased in network size from six stations to seven stations in 2003, then in 2011 to 9–10 stations and later in 2014 to eleven or more stations. The effect of these increases of network size is seen in the improvement of EOP formal uncertainties and precision discussed in Section 4. Fig. 3 shows how the number of network stations increased.

Fig. 4 displays the general increase in the number of observations per session for the R1 and R4 sessions since 2002. There is an increase in observations per session for the R1s that occurred in August of 2006 and then leveled off until 2013. The August 2006 increase is consistent with the replacement of tapes with disks as well as the increase

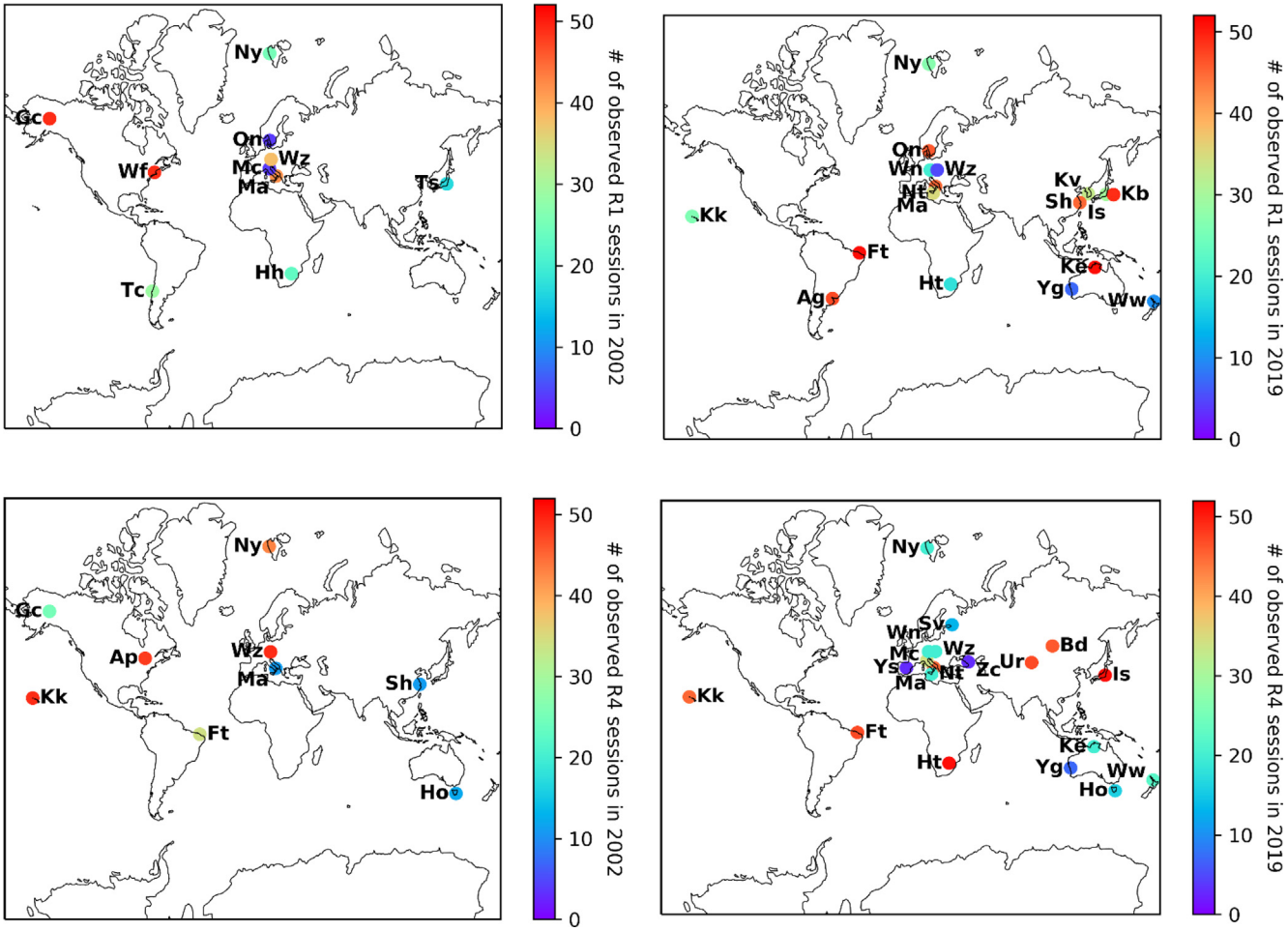

Fig. 2. Evolution of the R1 (top) and R4 (bottom) network sites from 2002 (left) to 2019 (right). The number of sessions observed by each site is indicated by the color bar.

in network size. Observations increased because tapes had required extra idle time for tape turn-around and tape change. Without this idle time requirement, more observations could be recorded. There is another increase starting in 2010 when AuScope stations were added to the R1 sessions. The number of observations continued to increase as Sejong was added to the network in Fall 2014. Yebes-13.5 m and Wettzell-North observed in *tag-along* (see Section 3.2) mode in 2015, but in 2016, Wettzell-North observed in standard mode. The increase in observations starting at the end of 2015 can be attributed to an increase in data rate from 256 Mbps to 512 Mbps for the even-week R1 sessions. The number of R4 observations increased steadily over time and the biggest increase came around mid-2014 to 2015. The increase is primarily due to decreasing the maximum scan length from 784 to 400 s and adding Wettzell-North and Yebes-13.5 m.

Fig. 4 shows that, although the number of observations increased over the years for both the R1 and R4 sessions, the number of observations that were used successfully (good observations) in data analysis decreased after 2016. The decrease in good R1 observations appears to be especially large since the beginning of 2016. Although the numbers of observations have increased dramatically over the years since 2002, the percentage of successful observations has not varied significantly. The ratio of successful R1 and R4 observations has not varied much, the average being about 80% of the observations scheduled from 2002 through 2017. Nevertheless, improving the success percentage needs to be further investigated. In 2018, we started using the source cull option (see section 3.3) when making the R1 schedule files and continue to use it. This command removes any source from the source list that had fewer than three scans. This increased the chance that the scheduled sources would be included in the final analyzed database. Although not significant, the gap between scheduled and used observations decreased starting in 2018.

3. Scheduling of sessions

3.1. Network construction

The process of constructing the different observing networks for the next calendar year begins in May of the current year. Each year the stations provide their availability, which is used to produce a Station Usage Chart that shows

Table 1
Statistics of stations and yearly number of sessions for the years 2002 (first R1 and R4 sessions), 2016 (largest station participation), and 2019 (latest year studied in this paper). The stations are ordered by decreasing latitude. The numbers in italics represent the number of stations participating per year in the Northern Hemisphere, the Southern Hemisphere, and globally. The numbers in bold indicate the stations that observed in more than 75% of the sessions for the year.

Station name					Yearly session number					
					2002		2016		2019	
2-letter	8-letter	Country	Lon.	Lat.	R1	R4	R1	R4	R1	R4
North		*Number of stations*			*8*	*7*	*11*	*12*	*11*	*13*
Ny	NYALES20	Norway	348.13	78.93	25	**43**	**45**	**45**	**45**	**44**
Gc	GILCREEK	USA	147.50	64.98	**49**	25				
Sv	SVETLOE	Russia	330.22	60.53				18		19
On	ONSALA60	Sweden	348.07	57.40	4		27		20	
Bd	BADARY	Russia	257.76	51.77				20		16
Wz	WETTZELL	Germany	347.12	49.15	**38**	**49**	**52**	**52**	**39**	**45**
Wn	WETTZ13N	Germany	347.12	49.15			24	23	28	27
Ap	ALGOPARK	Canada	78.07	45.96		**48**				
Mc	MEDICINA	Italy	348.35	44.52	4			13		12
Zc	ZELENCHK	Russia	318.43	43.79				19		20
Ur	URUMQI	China	272.82	43.47				6		5
Wf	WESTFORD	USA	71.49	42.61	**49**					
Ma	MATERA	Italy	343.30	40.65	**42**	11	21	22	29	19
Yj	RAEGYEB	Spain	3.09	40.52				1		
Ys	YEBES40M	Spain	3.09	40.52				21		15
Nt	NOTO	Italy	345.01	36.88					5	2
Kv	SEJONG	South Korea	232.70	36.52			**38**		**42**	
Is	ISHIOKA	Japan	219.78	36.21			25		**41**	**43**
Ts	TSUKUB32	Japan	219.91	36.11	17		**49**			
Kb	KASHIM34	Japan	219.34	35.96			2		4	
Sh	SESHAN25	China	238.80	31.10		11	15		17	
Kk	KOKEE	USA	159.67	22.13		**49**	20	**39**	37	**48**
South		*Number of stations*			*2*	*2*	*7*	*6*	*6*	*6*
Ft	FORTLEZA	Brazil	38.43	−3.88		34	**41**	**41**	29	**45**
Ke	KATH12M	Australia	227.85	−14.38			**39**	37	29	28
Hh	HARTRAO	South Africa	332.31	−25.89	23		6			
Ht	HART15M	South Africa	332.32	−25.89			15	16	**47**	**47**
Yg	YARRA12M	Australia	244.65	−29.05			**42**	**38**	**50**	**48**
Ag	AGGO	Argentina	57.93	−34.91					32	
Ww	WARK12M	New Zealand	185.17	−36.60			27	26	6	22
Tc	TIGOCONC	Chile	73.04	−36.82	29					
Ho	HOBART26	Australia	212.56	−42.80		12				2
Hb	HOBART12	Australia	212.56	−42.80			36	35		
Total number of stations					*10*	*9*	*18*	*18*	*17*	*19*

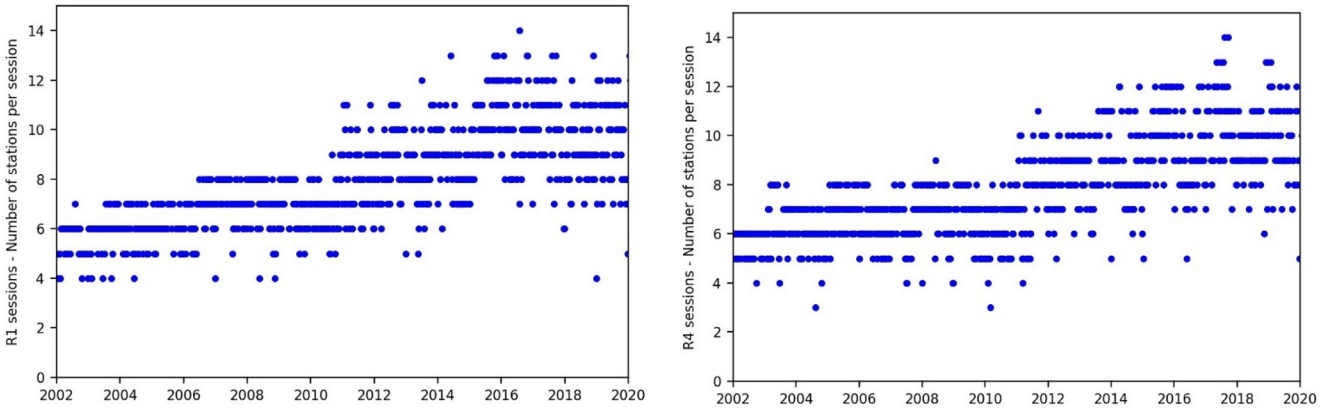

Fig. 3. R1 (left) and R4 (right) station numbers per session for the period of 2002 through 2019.

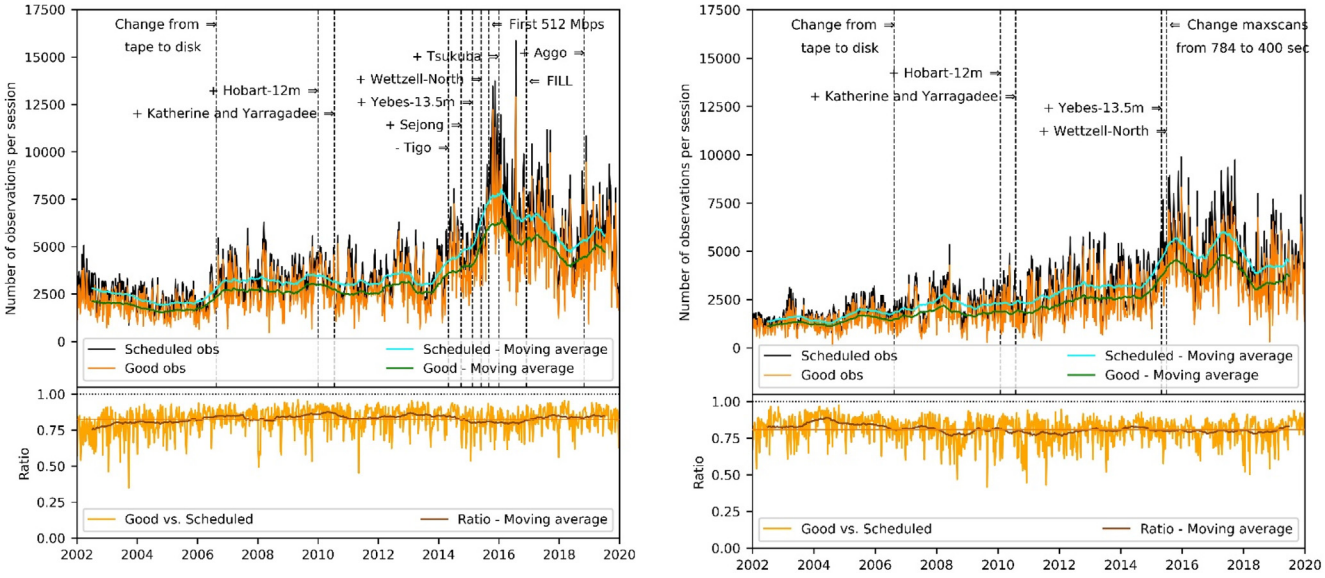

Fig. 4. R1 (left) and R4 (right) observation numbers per session for the period of 2002 through 2019. The average ratios of good versus scheduled observations are 0.8242 (R1) and 0.8094 (R4). Note: the scheduled numbers are adjusted to account for stations that did not observe the session.

how each station's availability is allocated to the different types of sessions. Station availability is based on a station's resources and other commitments. For the 52 R1 and 52 R4 annual sessions, station availability ranges from 5 to 52 observing days for both the R1 and R4 sessions. After the IVS Observing Program Committee (OPC) approves the allocation of station resources, a Draft Network Chart is produced. The R1 and R4 core station networks change each year based on station resources. A core network consists of a set of stations that can observe in every session. After the core network is determined, the remaining available stations are added to sessions during the year, which results in several different networks. Simulations are run for each possible R1 and R4 network to ensure each network produces good EOP results. Schedules are generated for different test network configurations. The scheduled observations are then run through analysis software that produces EOP estimates and uncertainties. Based on these results, the best network configurations are chosen. The original uncertainty goal in 2002 was 100 μas for polar motion and 3.5 μs (52.5 μas) for UT1 for the EOP of the R1 and R4 sessions. In 2019, the goal was to be below 55 μas for polar motion and 2.2 μs (33 μas) for UT1 when designing the networks.

Table 1 shows that some stations have participated in many more sessions than others. Stations that participated during a single year in at least forty of the weekly R1 or R4 sessions over the 2002–2020 period are Fairbanks, Algonquin, Westford, Matera, Wettzell, Kokee, Ny Alesund, HartRAO, Fortaleza, Sejong, TIGO, Tsukuba, Yarragadee, and Ishioka.

Both the R1 and R4 networks have had to be changed when certain stations became unavailable. Fig. 2 shows the effect of these stations on the geographic extent of the networks. For instance, during 2006 Algonquin participated in 27 R4 sessions before the Canadian government announced the cessation of operational VLBI activities on September 25. Algonquin suffered a major malfunction of the bearing assembly for the azimuth drive in August 2006 and there were no plans to repair the antenna (Berube and Searle, 2006). Fairbanks suspended operations at the end of 2005. More recently, Westford participated in most of the R1 sessions until it switched to VGOS observing in 2015.

There are three European VLBI Network (EVN) observing periods each year with a duration of three to four weeks. Care must be taken to ensure that there are one or more networks that can be scheduled during the EVN periods. Some of the stations that are not available during the EVN periods are Onsala, Urumqi, HartRAO-26 m, Svetloe, Badary, Zelenchukskaya, Medicina, Noto, Seshan, and Yebes. Fortunately, the problem of scheduling a globally distributed network during the EVN period decreased with the additions of HartRAO-15 m, the AuScope antennas and Warkworth. The problem is slowly returning because the AuScope antennas are switching to VGOS observing. Hobart-12 m last observed as an S/X station in June 2017 and Katherine in August 2019. The plan is for Yarragadee to switch to VGOS observing during the second quarter of 2022.

3.2. Scheduling program

The R1 and R4 session schedules were generated using the scheduling software program SKED (see Gipson, 2010; Gipson, 2012; Gipson, 2019). In this section, some of the parameters used to create these schedule files are discussed. Several typical session parameters at the beginning and end of the 2002–2020 period are given in Table 2.

Table 2
Typical session parameters.

Session	Date	Number of Scheduled Stations	Number of Sources	Data Rate [Mbps]	Min Scan Length [s]	Max Scan Length [s]	Minimum X/S SNR:Margin
R1001	2002–01-07	6	51	256	30	180	20/15:0/0
R4001	2002–01-03	6	62	56	98	784	20/15:5/3
R1920	2019–11-11	10	57	512	20	400	20/15:0/0
R4920	2019–11-14	11	100	256	60	400	20/15:5/3
R1921	2019–11-18	11	58	256	43	300	20/15:0/0
R4921	2019–11-21	12	100	256	60	400	20/15:5/3

The "Number of Scheduled Stations" column shows the number of stations scheduled but not all stations ended up in the database for various reasons. The SNR with a margin means a lower SNR target will be accepted within that margin.

We started using the stations Weights (statwt) command in 2004 for the R1 sessions. The command preferentially selects scans involving stations that are specified by the scheduler. Station weights are used in the R1 sessions to give higher weight to scans with less sensitive stations like TIGO, AGGO, and Fortaleza.

The Downtime Command (downtime) was used starting in 2006 to stop a station or stations from observing in a session for a specified period (Gipson, 2012). This command is used in the R1 and R4 sessions when stations stop observing to participate in a 1-hour UT1 Intensive session. For instance, the daily Intensive sessions with Kokee and Wettzell are scheduled at 18:30 UT with a duration of one hour. The downtime for Kokee and Wettzell is set for 18:15 UT to 19:45 UT during an R1 session. This downtime allows Kokee and Wettzell to leave the R1 to prepare for the Intensive session. Then it gives the two stations time to prepare to return to the R1 session.

The Early Start Parameter determines how early a station starts to record before the data is valid. This option was introduced for tapes which needed additional time for the correlators to synch up (Gipson, 2012). This parameter was not used for the R1 sessions after June 2008.

The new Fill Command (fill) was used in the R1 sessions for the first time in January 2017 for the R1773 session. The Fill Command increases the duration of scans, when possible, to decrease the idle time for each station. More recording media is used due to the longer scan lengths, but it improves the SNRs on the affected baselines.

The *tag-along* mode of scheduling a station is used to add a station returning from major repairs or a new station to an observing session without affecting the scheduled observations of the original network. After a schedule has been generated, observations with the additional station are added but without affecting the originally scheduled observations. For instance, observations of a source in a specific scan could be augmented with possible observations using the additional station.

3.3. Source selection

The set of VLBI radio sources to be scheduled in the R1 and R4 sessions are selected from two different sets: the good geodetic source catalog and the monitoring source list. At the beginning of the R1 and R4 observing program, the good geodetic source catalog was built from an initial set of radio sources considered suitable for geodetic observations. These radio sources were 1) strong (flux densities larger than 0.1 Jy), allowing for shorter integration times so that more observations can be scheduled, 2) compact or point-like such that their flux density was nearly constant for all baseline lengths, and 3) free of significant radio source structure that could introduce observation noise (Gipson, 2010; Gipson, 2019). Recent studies (Anderson & Xu, 2018; Xu et al., 2021) have demonstrated that sources in this catalog have shown source structure that causes significant impact on long baselines, leading to the conclusion that these sources do not fulfill the conditions of the initial selection. However this catalog is still used to schedule R1 and R4 sessions.

The current good geodetic source catalog is reviewed and updated at GSFC/NASA. In May 2020, it contained 336 sources: more than 97% (95%) of geodetic sources have X-band (S-band) fluxes > 0.1 Jy; more than 87% (78%) of sources have X-band (S-band) fluxes > 0.2 Jy. The catalog is available on https://github.com/nvi-inc/sked_catalogs/.

Two conditions for an optimal geodetic schedule are that the schedule contains strong radio sources and that these sources are well distributed over the sky (Gipson, 2019). The first condition is fulfilled by using the set of sources in the good geodetic source catalog as the foundation set of sources. To generate a schedule with good sky coverage for each session, the Sked command *bestsource* is used with an integer argument for the number of sources to observe in a session. Sked selects the chosen number of sources that will give the best sky coverage, depending on the stations that are observing and the start and stop time of the session. There are other sked commands that influence sky coverage. *MinBetween* sets the minimum time between observations of the same source. *TimeWindow* sets the time window (hours) used in computing sky coverage.

From March 2004 for the R1 sessions (R1114 and later) and from July 2010 for the R4 sessions (R4437 and later), the R1 and R4 sessions participated in the NASA GSFC VLBI Group's Source Monitoring Program (Gipson et al., 2014). Beginning in June 2003, the VLBI Group developed a database to monitor radio sources of interest associated with an annual observation target for each of

the sources. The database records information on each source for each IVS session, such as the number of sessions in the past twelve months each of the sources of the monitoring program was successfully observed in. The Sked command *monitor* is called with an integer argument for the number of sources to find in the search of the database for the least observed sources in the Source Monitoring Program. The primary goal of the monitoring program is to increase the observations of sources that do not reach their observation target. In R1 and R4 sessions, there are up to ten sources selected from the Source Monitoring Program database. This number was chosen to not significantly degrade the measurement of the EOP, which is the primary purpose of these sessions.

The optimal number of sources scheduled in a session depends on different factors. First and foremost, a source must be observed a satisfactory number of times and for sufficiently long scan times to help ensure the success of the observations. Sources should be observed on several scans during the experiment and possibly by sets of three or more antennas to strengthen the source position determination. The second factor regarding selecting the optimal number of sources comes from technical aspects of the schedule, such as the recording rate, the sensitivity of the antennas, and the station data storage capacity. Higher recording rates, higher antenna sensitivity and larger storage capacity will allow for more scans and the possibility of observing more sources. As seen in Fig. 5, the R1 and R4 scheduling strategies yielded numbers of session sources that evolved between 2002 and 2020. The numbers of sources scheduled and used in the VLBI global solution (named "good") are shown in these plots. It is important to mention that the numbers of scheduled sources are adjusted to account for the stations that did not observe. This means that in the case a station was initially scheduled in the observing network but could not participate, the numbers of scheduled observations corresponding to this station are removed from this analysis.

For the R1 sessions from 2003 to 2009, the selection of sources is very homogeneous from one session to the next. The best 50 sources associated with the session station networks were selected from the good geodetic catalog as well as up to ten sources from the source monitoring program radio source catalog. The strategy gave a regular set of about 60 sources that were optimally scheduled as seen by the success ratio between the number of sources used in the global solution and the number of scheduled sources, where the ratio is close to one. However, near the end of 2009, for every session, there are between five and ten sources that are scheduled but not used. This can be attributed in part to unexpected changes in the structure of some of the sources in the good geodetic source catalog. In mid-2015, a modified strategy was tested, where the number of sources scheduled was increased to 90. After re-evaluation, between 70 and 80 sources per session were scheduled from 2016. Beginning in July 2018, the strategy for selecting the number of sources in R1 sessions was optimized to have all the scheduled sources observed on a satisfactory number of scans, using the *source cull* command of Sked. Each scheduled source was required to be observed at least three times. The success ratio becomes closer to one and comparable to the performance from 2005 to 2008. In mid-2019, the number of sources decreases to between 48 and 67 sources based on using the source cull command.

For the R4 experiments, there is a clear increase in the number of sources beginning in July 2010, when these sessions entered the Source Monitoring Program (see above). The strategy in the selection of sources evolves from about 60 sources in mid-2010 to about 90 sources in mid-2015. In mid-2015, the Sked schedule parameter maxscan is reduced. This parameter specifies the longest scan allowed. If maxscan decreases, the number of observations increases as seen in Fig. 4 as well as the number of scans, which can lead to an increase in the number of sources used. The success ratio is not as close to one as for the R1 experiments, indicating there may be too many sources scheduled.

4. Analysis

4.1. EOP uncertainties from the R1 and R4 sessions

The VLBI analysis in this paper was performed with the Calc/Solve analysis program. Ma et al. (1990) includes a general description of the Solve least-squares estimation program and the theoretical models that are most commonly applied. Generally, the theoretical models employed follow the recommendations of IERS Conventions 2010 (Petit et al., 2010). The VLBI terrestrial reference frame (TRF) solutions used for this paper estimated global and session parameters. Global parameters are based on the entire observing period of VLBI daily sessions. These parameters are site positions, site velocities, and radio source positions. The site positions and velocities were constrained to ITRF2014 (Altamimi et al., 2016) via NNR and NNT constraints and radio source positions to ICRF2 (Fey, 2015) defining source positions via a NNR constraint. This method of analysis ensures the stability of the reference frame based on the entire data set and the consistency of the estimated parameters with the reference frame. Session parameters are based on observations only within each VLBI 24-hour session. These include polar motion and their rates, UT1, LOD, nutation, site wet zenith delays, site troposphere gradient delay parameters, and site clock parameters. Observations within each session used session weight factors derived from independent analysis of each session where observation sigmas have been weighted to make the χ^2 per degree of freedom of the observation residuals equal to 1. Baseline weighting adds a constant noise term in quadrature to the correlator observation sigma to compute the session residuals for each baseline. This analysis is first conducted after each session

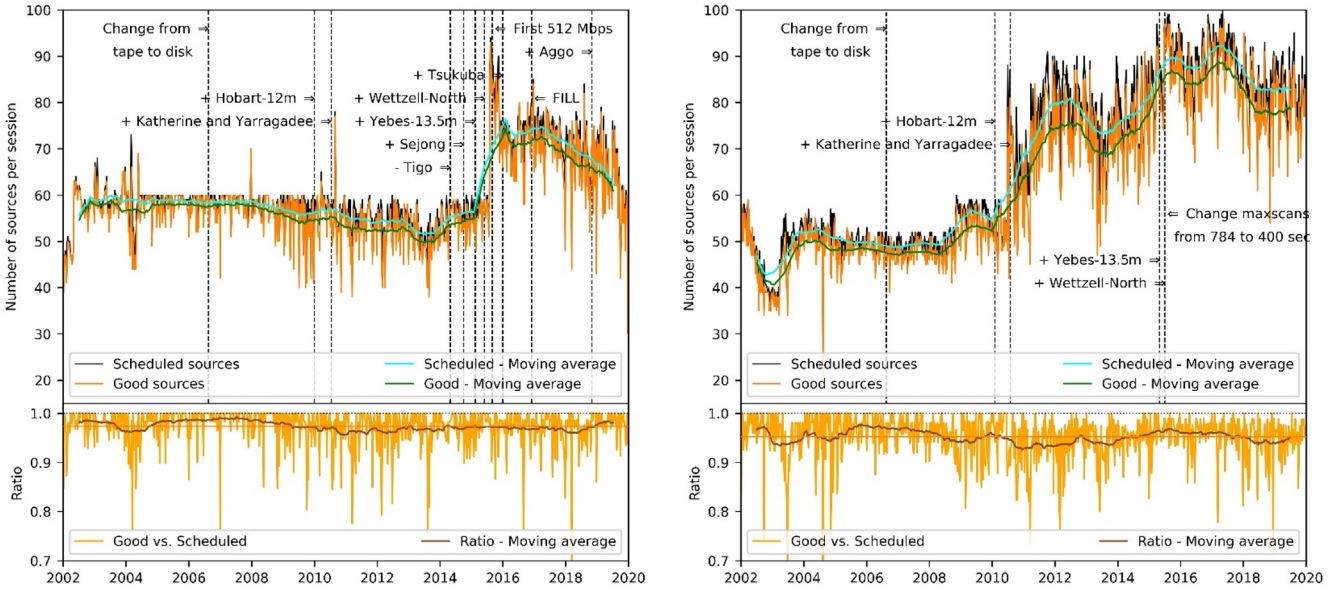

Fig. 5. Evolution of the number of sources in the R1 experiments (left) and the R4 experiments (right) that were scheduled (black) and used in the VLBI global analysis solution (orange). The moving averages (1-year window) are shown respectively in light blue and yellow. The average ratios of good versus scheduled sources are 0.9725 (R1) and 0.9508 (R4). Note: the scheduled numbers are adjusted to account for stations that did not observe the session.

is observed, although all weights are generally recomputed in later analysis.

Standard TRF solutions as described above make global estimates of station positions and velocities and estimate EOP on a session-by-session basis using the global estimates. EOP estimates determined from such a solution were used to compare with GNSS EOP estimates in Sec. 4.3. Because velocities were estimated, the uncertainties in the reference frame propagate into the EOP uncertainties. The reference frame has the best uncertainty in the middle of the data span of the sessions in the solution and increases towards the ends. Because of this, even if the network and observing schedules remained the same, the EOP uncertainties would be larger towards the ends of the observing span. An alternative way of studying the EOP uncertainties is to turn off reference frame change by not estimating station velocities. This alternative no-velocity solution is identical to a standard TRF solution except that velocities are not estimated but instead are fixed to the a priori velocities, which in this case are aligned with ITRF2014. This solution was run only for the purpose of studying the evolution of EOP uncertainties. The resulting EOPs are only influenced by each observing session and allow a truer comparison of EOP uncertainties at different epochs. In the IVS WG2 Final Report, Schuh et al. (2002) discussed the goals of IVS VLBI observing and laid out goals for parameter estimate uncertainties. At the time, average UT1 uncertainties were about 5 μs (75 μas) and X and Y polar motion uncertainties were 100 μas and 200 μas, respectively. The IVS EOP uncertainty goal was to improve the uncertainties by a factor of 2 to 4. As shown in Fig. 6, the formal uncertainties have met this goal.

Fig. 6 shows that the R1 EOP formal uncertainties without velocity estimation improved from 2002.0 to 2020.0. The X-pole and Y-pole uncertainties for the R1 sessions improved by factors of 3 and 2 and UT1 by a factor of about 1.2. The moving median (one year window) trend lines for R1 pole position uncertainties decreases from 60 μas in early 2002 to 20–25 μas in 2017. The moving average shows a small linear trend. There is a larger improvement for the R4 sessions where X-pole improves by a factor of 3.5 and Y-pole improves by a factor of 2.4. UT1 improves by a factor of 1.6. The moving average trend line for R4 X-pole position improves from 80 μas in early 2002 to 20 μas in 2017 and from 60 μas in early 2002 to 25 μas in late 2017 for Y-pole. The UT1 uncertainties improve from 2.7 μs (40 μas) to 1.7 μs (25 μas). The main reason for these improved EOP uncertainties was the increase in network size of both R1 and R4 sessions, which produced more observations and better global network geometry shown in Fig. 2 and discussed in Section 2.2. In the next section, we investigate in more detail the reasons that these EOP uncertainties have improved.

4.2. Improvement of EOP uncertainties

In this section, we consider the significance of several factors that could have contributed to the improvement of EOP precision. These factors are 1) increase in network size, 2) changes in data rate, and 3) increase in the number of sources in each session.

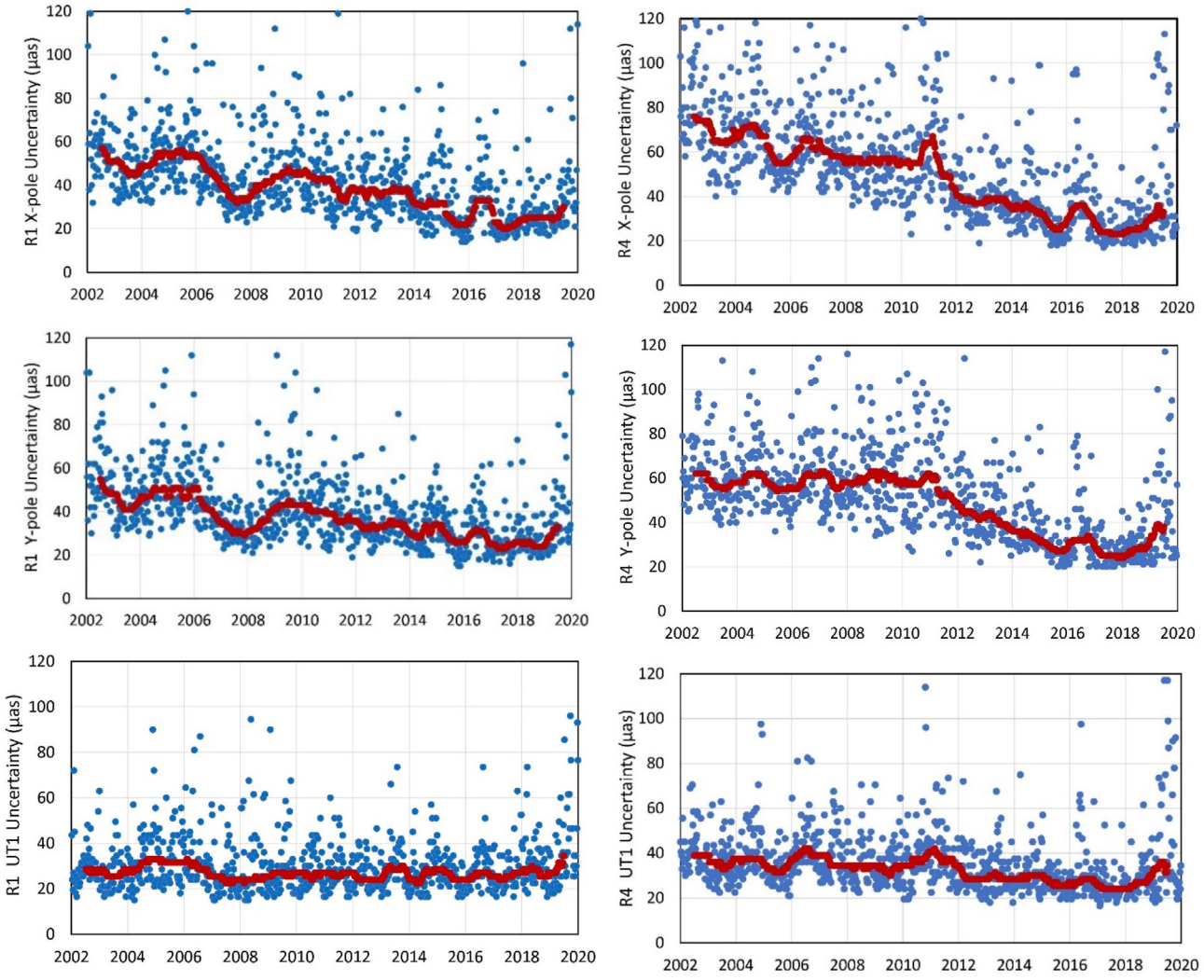

Fig. 6. R1 (left) and R4 (right) X-pole, Y-pole, and UT1 formal uncertainties estimated without estimation of velocities in the TRF solution, where the conversion factor of 15 from µs to µas was applied for UT1 to allow comparison with polar motion precision. The smoothed red curve in each plot is the median uncertainty computed at each epoch using a one-year window.

4.2.1. Network size

We begin by looking at the sensitivity of the VLBI delay to rotations. The delay is

$$\tau = -\overrightarrow{B} \cdot \hat{s} \tag{1}$$

where $\overrightarrow{\boldsymbol{B}}$ is the baseline vector and $\hat{\boldsymbol{s}}$ is the unit vector in the observed source direction (declination θ and right ascension φ)

$$\hat{s} = (cos\theta cos\varphi, cos\theta sin\varphi, sin\theta) \tag{2}$$

Rotation is given by a vector $\overrightarrow{\omega}$ where the components are rotations about the X, Y, and Z axes. With an infinitesimal rotation corresponding to $\overrightarrow{\omega}$, the change in the baseline vector is

$$\Delta\overrightarrow{B} = \omega \times \overrightarrow{B} \tag{3}$$

$$\Delta\tau = -\overrightarrow{\Delta B} \cdot \hat{s} \tag{4}$$

$$\Delta\tau = -\overrightarrow{\omega} \cdot \overrightarrow{B} \times \hat{s} \tag{5}$$

The sensitivities of the delay to the components of $\overrightarrow{\omega}$ are the partial derivatives

$$\frac{\partial\tau}{\partial\overrightarrow{\omega}} = \hat{s} \times \overrightarrow{B} \tag{6}$$

$$\frac{\partial\tau}{\partial\overrightarrow{\omega}} = \left(B_z cos\theta sin\varphi - B_y sin\theta, B_x sin\theta - B_z cos\theta cos\varphi, B_y cos\theta cos\varphi - B_x cos\theta sin\varphi\right) \tag{7}$$

The sensitivity to ω_i will be zero for a baseline (or baseline component) aligned with the i^{th} rotation component axis. The greatest sensitivity will be for baselines perpendicular to this axis. For instance, long baseline projections on the X-Y equatorial plane provide the maximum sensitivity to UT1. This is why one-baseline Intensive sessions dedicated to UT1 determination generally use such baselines.

Long baselines should in principle provide the greatest sensitivity to rotations. However, as baseline length

increases, the possible source sky coverage (available visibility solid angle) for observations decreases from full sky coverage for near zero length baselines to no possible observations for baselines with length equal to the diameter of the Earth. For instance, in the R&D CONT17 sessions, baselines of length less than 2000 km had 4000 to 6000 observations and baselines longer than 10,000 km had 100 to 1000 observations (MacMillan, 2022). Therefore, it is a combination of optimal baseline length and sky coverage that yields the best sensitivity to rotations and the best resulting EOP precision.

EOP uncertainties will vary inversely with the number of observations

$$\sigma_{EOP} \sim 1/L\sqrt{numobs} \tag{8}$$

and a length L that characterizes the size of the network that contributes to a given component of EOP.

The normal matrix

$$N = \left[\frac{\partial \tau}{\partial \vec{\omega}}\right]^T W \left[\frac{\partial \tau}{\partial \vec{\omega}}\right] \tag{9}$$

reduces to a sum over the observations because the weight matrix W is diagonal with elements equal to the inverse of the square of the observation sigmas. If we have many baselines in a session, then the normal matrix for the session will then be the sum of the normal matrices for all the baselines observed in a session

$$\boldsymbol{N} = \sum_{baselines\ j} N_j \tag{10}$$

The formal uncertainties for $\vec{\omega}$ are diagonal elements of the inverse of the normal matrix.

We consider the special case of baselines in the X-Z plane aligned with the z-axis to understand the dependence of the formal uncertainties on baseline lengths and the number of observations made in a VLBI session. Gipson (1998) discussed some similar cases in a memo on baselines and EOP. In our special case, the entire baseline is projected into the X-Z and Y-Z planes. For this example, only polar motion and UT1 are estimated. The normal matrix is much easier to evaluate. The general case of an arbitrary baseline between two stations on the Earth is more complicated to evaluate. Such baselines will yield polar motion information but no UT1 information.

$$\frac{\partial \tau}{\partial \vec{\omega}} = (B_z cos\theta sin\varphi, -B_z cos\theta cos\varphi, 0) \tag{11}$$

It will be assumed for this exercise that the observation sigmas are constant, whereas in fact they depend on various station details including mainly the sensitivities of the baseline stations.

$$N_{xx} = B_z^2 \sum_{obsi} f(\theta_i, \varphi_i) \frac{1}{\sigma_i^2} \tag{12}$$

where $f(\theta, \varphi) = (cos\theta sin\varphi)^2$. If we assume that the observations are uniformly distributed over the mutual visibility region of the sky and that the observations all have the same uncertainty σ, this can be written

$$N_{xx} = B_z^2 \frac{Numobs}{\sigma^2 \int d\Omega} \int f(\theta, \varphi) d\Omega \tag{13}$$

The integral is normalized by the factor Numobs/mutual visibility solid angle. Define the factor

$$F = \frac{1}{\int d\Omega} \int f(\theta, \varphi) d\Omega \tag{14}$$

A vertical baseline extends from the Southern to Northern Hemispheres such that there is an angle α between the station radial vectors. This angle increases from 0 to π as the baseline length increases from 0 to twice the Earth's radius where the mutual visibility solid angle vanishes. One can then evaluate the normal matrix element N_{xx}

$$N_{xx} = \frac{B_z^2 Numobs}{\sigma^2} F \tag{15}$$

In this case, F = 1/3 but if we had chosen the baseline to be in the Y-Z plane again aligned with the z-axis, then

$$F = \frac{1}{3}\left(1 - \frac{\sin\alpha}{\pi - \alpha}\right) \tag{16}$$

F decreases from 0.27 to 0.15 over the range baseline lengths from 3000 km to 8000 km. For the CONT17 sessions mentioned above that used a network similar to the largest R1 and R4 networks, 77% of the observations were made in this range of baselines.

For the x-component of polar motion, the session normal matrix in Eq. (9) becomes

$$N_{xx} = \sum_{baselines\ j} N_{j,xx} = \frac{obs_{tot}}{\sigma^2} \sum_{baselines\ j} \frac{obs_j}{obs_{tot}} B_{jz}^2 F_j \tag{17}$$

where obs_j is the number of observations on the jth baseline and obs_{tot} is the number of session observations. Depending on the baseline, the factors F_j vary with baseline length but we assume for this exercise that they are equal to a constant value.

$$N_{xx} = \frac{obs_{tot}}{\sigma^2} \left[B_z^2\right]_{avg} \tag{18}$$

In general, the formal uncertainty of ω_x is the first diagonal element of the inverse of the normal matrix

$$\sigma_x = \sqrt{\left(N^{-1}\right)_{xx}} \tag{19}$$

where as, in the special case here, the uncertainty is the reciprocal of $\sqrt{N_{xx}}$. The characteristic baseline length is then

$$L = \sqrt{\left[B_z^2\right]_{avg}} \tag{20}$$

In this special case, L equals the projected baseline lengths onto the X-Z plane.

The approximate EOP uncertainties shown in Fig. 7 for the R1 and R4 sessions are based on the approximate relation in Eq. (8). For UT1, X-pole, and Y-pole, L is the aver-

age projection of the baseline lengths in each session, on the equatorial X-Y plane, the X-Z plane, and the Y-Z plane, respectively. In computing these averages, the squares of the projected baseline lengths are weighted by the number of observations made on the baseline. This weighting is done to account for the fact that the number of observations decreases with baseline length due to reduced available sky coverage. The models were scaled to make the initial model uncertainties after 2002.0 roughly agree the corresponding X-pole, Y-pole, and UT1actual formal uncertainties: R1 (57 μas, 55 μas, 29 μas) and R4 (76 μas, 62 μas, 39 μas) in Fig. 6. The evolution of these approximate uncertainties in Fig. 7 are similar in terms of the general trends and specific short-term features to that of the actual uncertainties in Fig. 6.

The average baseline projections for each R1 and R4 session vary over the period from 2002.0 to 2020.0 depending on stations being added or sometimes removed from networks but there is not a clear overall increase in these average length projections over this period. Average baseline projections for the R1s and R4s have similar variability: X-Z plane (5000–7000 km), Y-Z plane (4000–6000 km), X-Y plane (4500–6500 km). Systematic changes in the average lengths of baseline projections (due to changes in network stations) cause some systematic changes in the EOP uncertainties. For instance, the average R4 Y-Z projection (Y-pole) decreases from 2008 to 2010.5 from about 4500 km to 3500 km, but thereafter increases to 5000 km at 2020.0. This behavior contributes to the apparent flattening of the uncertainty trend before 2011.0.

The number of R4 baselines increased from 20 ± 10 baselines in 2011 (5–8 stations) to 40 ± 20 baselines (8–12 stations) in 2017.0, thereby significantly increasing the number of session observations. The corresponding increase in the number of stations is shown in Fig. 3. There was a similar increase in the number of R1 baselines around 2011.0 that similarly led to a decrease in polar motion uncertainties.

The general improvement of the uncertainties in Fig. 7 is due mainly to the increase in the number of observations caused by the increase in the number of network baselines. This is clear from Fig. 8, which shows that the number of observations per session generally increases with the number of baselines in a network. A network with N stations has N (N-1)/2 baselines. Obviously, only requiring a network to have many stations will not yield superior EOP uncertainties. The R1 and R4 networks also have long baselines.

The increase in the X-pole and Y-pole uncertainties in 2016 is consistent with a reduced number of observations shown in Fig. 4 for both the R1 and R4 sessions. The R1 and R4 EOP uncertainties appear to be leveling off in 2017–2018 and increasing in 2019. This is most likely due to network station availability issues that affect the global distribution of sites and the number of observations in a 24-hour session. It can be seen in Fig. 3 that there is a decline in the number of stations in the R1 networks after 2017.0. Hobart-12 m stopped observing in both networks and Warkworth-12 m ended its observing in the R1s. Fig. 4 shows that the number of R4 observations has decreased significantly since 2017.0, which leads to higher EOP uncertainties seen in Fig. 6.

Malkin (2009) showed that in general EOP formal uncertainty (referred to there as precision) and the WRMS difference with respect to IGS EOP (referred to as accuracy) improves as the network volume increases. This volume is a measure of the combined effect of the number of stations in a network and its global distribution. Malkin analyzed EOP series for the period July 1996 until February 2007. This period covers at most 5 years of the R1 and R4 series. Nothnagel et al. (2017) also shows that the formal uncertainties improve with larger network volume. These investigations do not attempt to analyze the evolution of the R1 and R4 series and the corresponding improvement in the precision of estimated EOPs. They also do not investigate how the volume evolves in time.

4.2.2. Observation data rate

One might argue that the observation data rate could be a factor in the improvement of EOP formal uncertainties. A higher data rate should allow more observations to be made and thereby improve the precision of EOP estimates. The data rate for the R1 series has been 256 Mbps since the series began except for a test period from 2015 to 2019 in which the even-numbered sessions were observed at 512 Mbps. However, most of the improvement for the R1 series occurred before 2015 indicating that the data rate is essentially not a factor for improvement.

The R4 data rate was 256 Mbps from August 2009 through 2020 (and to the present). Before this, the data rate increased from 56 Mbps starting in 2002. The main decrease (improvement) in X-pole uncertainty before August 2009 occurred during the period when the data rate was 56 Mbps. Fig. 7 shows that the number of R4 observations was significantly less than the number of R1 observations from 2002 to 2006. This could have contributed to the larger X-pole R4 uncertainties. There is not a clear decrease of the trends of the Y-pole or UT1 uncertainties before 2010 when data rates were increasing. This implies that the data rate was not a factor in the improvement of the uncertainties. (See the history of data rates in Table 3).

4.2.3. Number of sources observed

Another possible contributing factor to the improvement of EOP formal uncertainties is the number of sources that are observed in a session, which is shown in Fig. 5. The number of sources per R1 session was nearly unchanged from 2002.0 until 2015.0 varying from 55 to 60 sources. Most of the improvement in EOP uncertainties took place during this period. After 2015.0, the number of sources increased to about 75 but then decreased from 2017.0 to 48–67 sources. This brief period of more observed sources does not appear to have affected the EOP uncertainties.

On the other hand, the variation in sources per session for the R4 series is more complicated. Until 2008, about

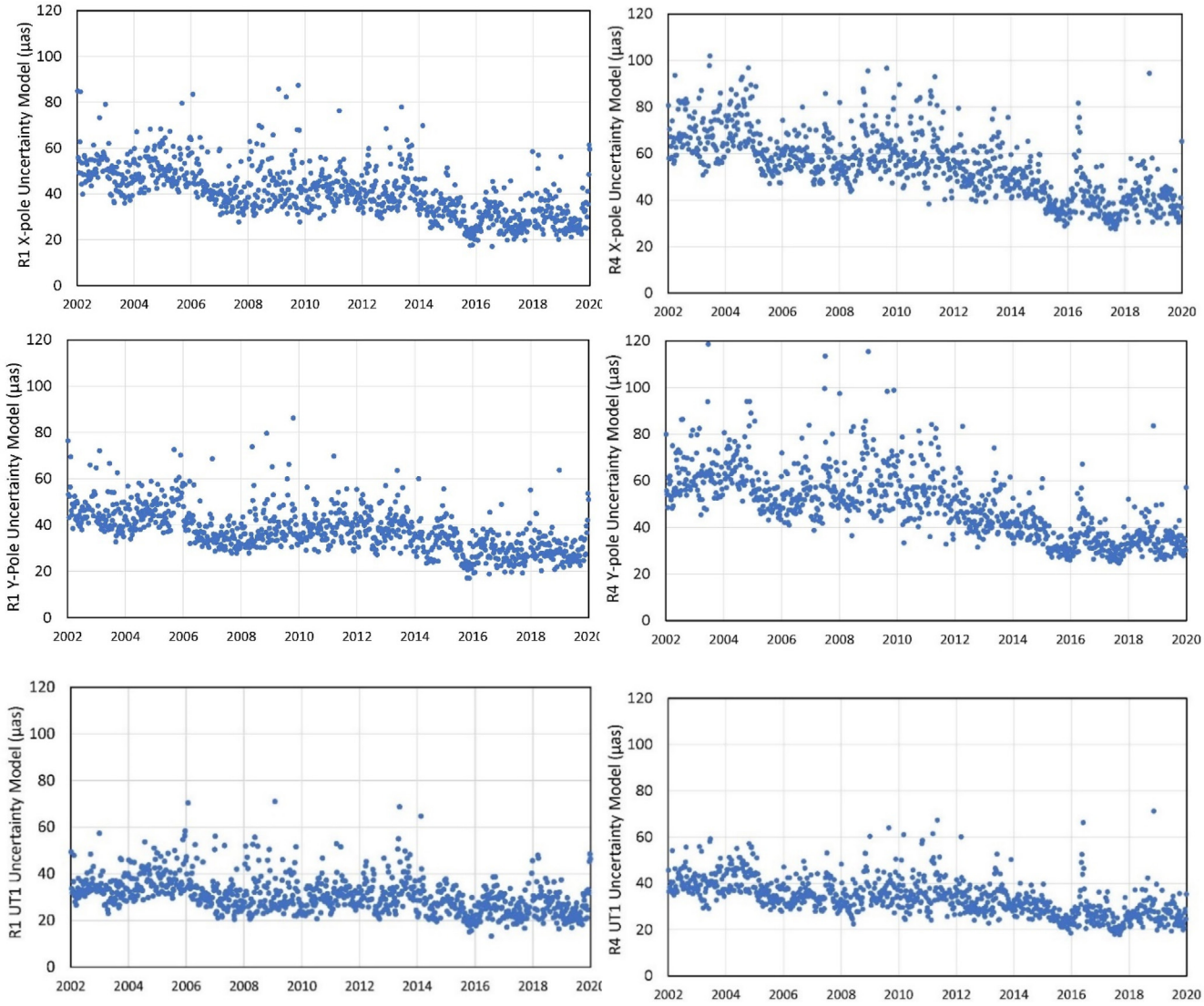

Fig. 7. R1 (left) and R4 (right) X-pole, Y-pole and UT1 uncertainties modeled as a function only of the number of observations and the average projected baseline lengths for each EOP component for each session.

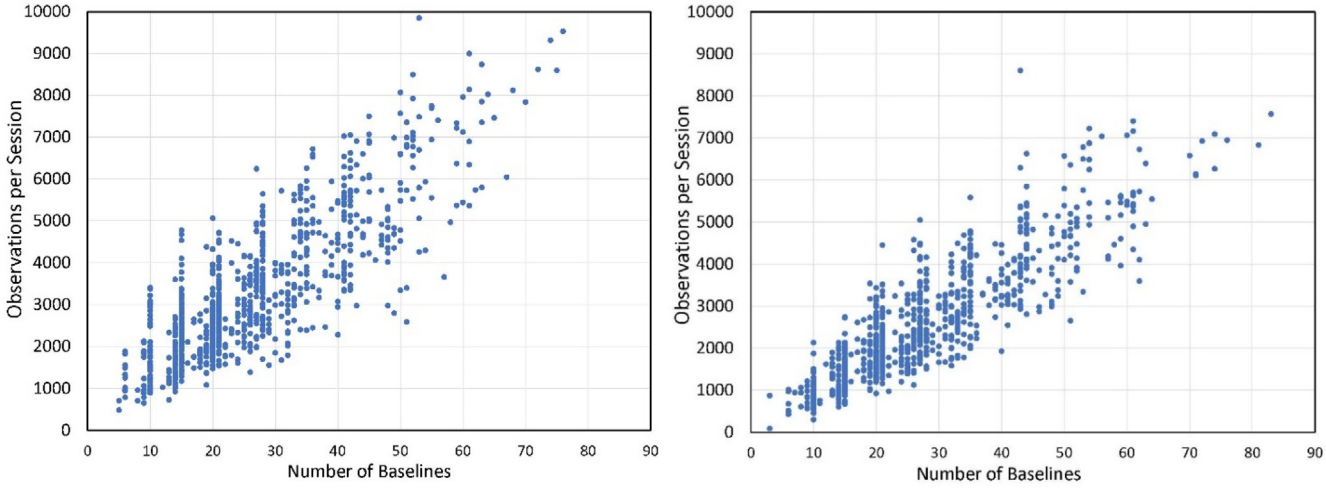

Fig. 8. R1 (left) and R4 (right) observations per session as a function of the number of baselines in the session.

Table 3
Data Rates.

	56 Mbps	112 Mbps	128 Mbps	256 Mbps	512 Mbps
R1				2002–2020 2015–2019 Odd sessions	2015–2019 Even sessions
R4	1/2002 to 11/2005	11/2005 to 1/2007	1/2007 to 8/2009	8/2009 to Present	

50 sources per session were observed. From 2008 until about 2017.0, there was a general increase to 90 sources per session. One could argue that the increase in number of sources is correlated with the improvement in the EOP uncertainties that can be seen after 2010.0. However, based on the network analysis above, the improvement is explained by the increased number of observations due to the increase in the number of R4 baselines. In addition, typically, when 80–90 sources were observed in R4 sessions, 10–15% of the sources were observed less than 3 times. Relevant questions are 1) what is the optimum minimum observations per source and 2) what is the effect on parameter estimates arising from observations of some sources only a few times. On the other hand, it could be desirable to observe these sources to improve their precision in the celestial reference frame.

4.3. Comparisons with GNSS polar motion

Since VLBI and GNSS are independent geodetic techniques, differencing common estimated parameters like polar motion can reveal systematic differences between the techniques. To compare VLBI and GNSS polar motion, we used a reprocessed GNSS series (courtesy of Paul Rebischung, IGN, 2022). This series was computed with the same reference frame IGSR3 from 1995 to 2021. On the other hand, the IGS Finals series (Dow et al., 2009) was not created entirely with the same reference frame throughout. The VLBI series was generated with a standard TRF solution as described in the previous section where velocities are estimated. The GNSS EOP series was interpolated via cubic spline interpolation to the epochs of the VLBI estimates. Each VLBI EOP epoch is at the midpoint (about 18 UT for most VLBI sessions) of each observing session where the precision of VLBI estimates is the best. We then computed the differences between the VLBI and GNSS series of polar motion estimates. The uncertainties of the differences were computed as the square root of the quadratic sum of the VLBI and GNSS uncertainties. The polar motion GNSS formal uncertainties ranged from 5 μas in 2002 to 3 μas in 2020. Since the reference frames of the VLBI and GNSS techniques are not the same, there will be inherent biases between polar motion estimated by the two techniques. The difference series were detrended by removing an offset and rate for the overall period of R1 and R4 observing from 2002.0 to 2020.0. This procedure was carried out for each component of polar motion of each of the R1 and R4 series.

Fig. 9 shows the X-pole and Y-pole R1 and R4 detrended differences between the R1 series and the R4 series, respectively, and the reprocessed GNSS series. These difference series were detrended by removing an overall offset and rate over the period 2002.0–2020.0. The differences were then smoothed with a running 1-year window. The smoothed curves for the R1 differences in Fig. 9 were superimposed on the R4 plots in Fig. 9 to show how similar they are despite the fact that the R1 and R4 series are independent VLBI session series using different networks. There is some overlap of stations employed in the R1 and R4 network series, but it appears likely that the similarities reflect systematic behavior of the GNSS series. The RMS of this variation is a measure of the combined accuracy of the two techniques.

There are systematic variations between VLBI and GNSS polar motion, but it is also of interest to see how the relative precision of VLBI and GNSS evolves. For each 1-year window, we computed the weighted root-mean-square (WRMS) of the differences with respect to the mean difference in that window. This WRMS and the mean difference were each computed using formal uncertainties equal to the VLBI and GNSS uncertainties added in quadrature. The variance σ^2 of the differences is just the $WRMS^2$ of the residual differences.

$$WRMS^2 = \sigma^2\left(x_{vlbi} - x_{gnss}\right) \tag{21}$$

One measure of polar motion precision is the WRMS difference between VLBI and GNSS estimates. This measure of precision is different from the formal precision or formal uncertainty discussed in the previous sections in the sense that it evaluates the actual polar motion estimates based on real observations. Accuracy refers to how close measurements are to some accepted value; whereas, precision refers to how close measurements of the same quantity are to each other. In the present case, the WRMS is a measure of the combined precision of the two techniques to measure the same polar motion variable. The bias between the two techniques is the only measure of accuracy available However, it is apparent from Fig. 9 that the bias does vary over the course of the R1 and R4 observing. One could interpret the variability of the bias as a measure of accuracy.

Since the VLBI and GNSS measurements are independent, they are uncorrelated. We compared the VLBI and GNSS estimates of EOP where the offset and rate biases between the entire series have been removed. Then the variance of the differences in each 1-year interval is the sum of

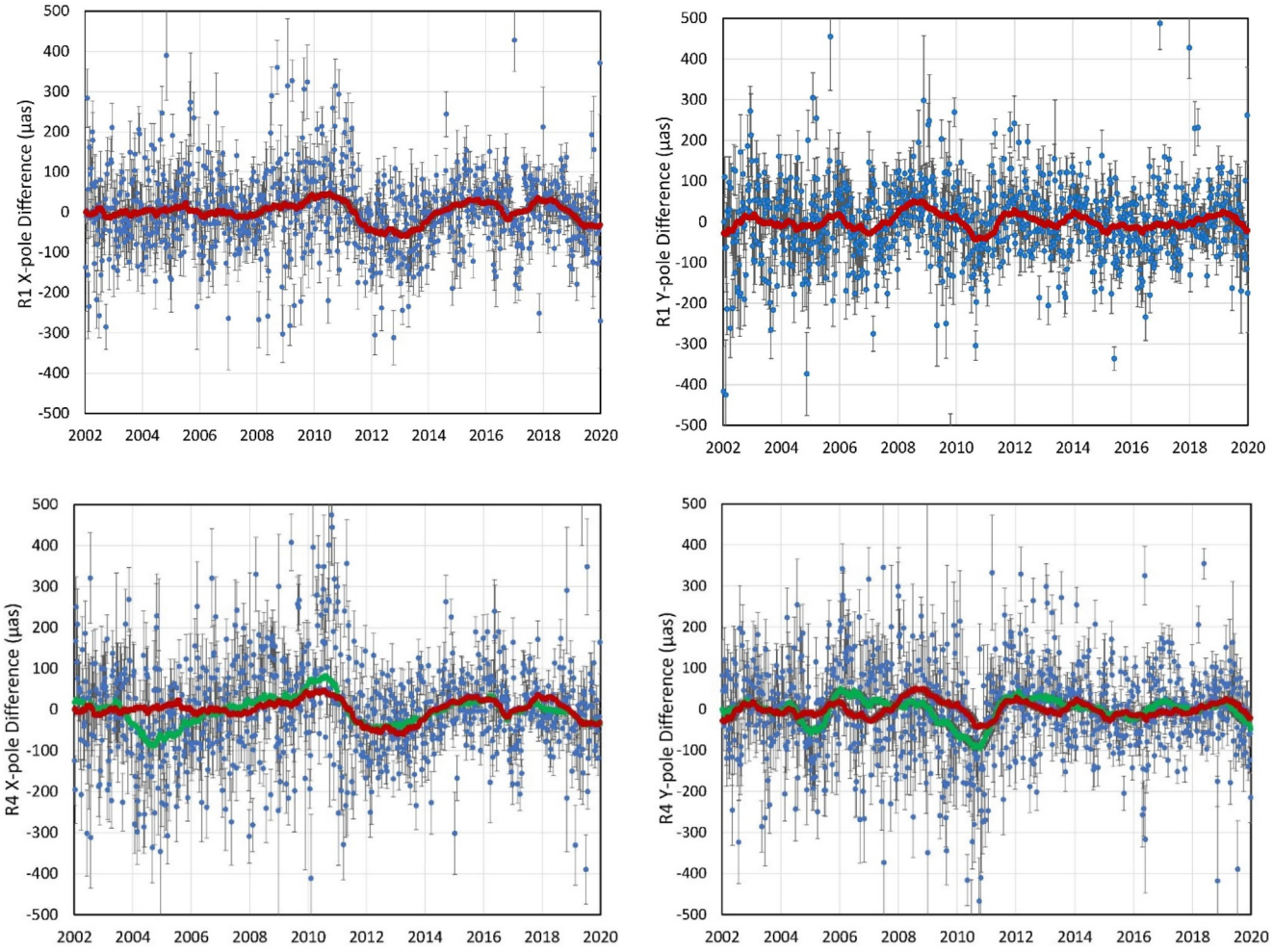

Fig. 9. X and Y polar motion differences (top figures) between estimates from R1 sessions and the IGS series. The differences were smoothed with a moving 1-year window to generate the R1 red curves. Polar motion differences for the R4 sessions appear in the lower plots where the smoothed curve is green for the R4 differences. The corresponding R1 smoothed red curves are shown here for comparison.

the unknown variances of the VLBI and GNSS series minus a term proportional to the covariance between the two series

$$\sigma^2(x_{vlbi} - x_{gnss}) = \sigma^2(x_{vlbi}) + \sigma^2(x_{gnss}) - 2Cov(x_{vlbi}, x_{gnss}) \quad (22)$$

The unknown variances are the squares of the unknown VLBI and GNSS intrinsic precisions in the 1-year interval. Since the VLBI and GNSS estimates are independent, the last term vanishes leaving

$$WRMS^2 = \sigma^2(x_{vlbi}) + \sigma^2(x_{gnss}) \quad (23)$$

If the GNSS and VLBI precisions were the same, then that precision would be equal to $WRMS/\sqrt{2}$. Given that the GNSS network has hundreds of receiving sites compared with VLBI R1 or R4 networks that have at most 14 sites which vary between networks, the precision of GNSS should be better than the precision of VLBI. The large number of GNSS sites results in a more stable network than VLBI. Removing GNSS sites or replacing sites does not affect the overall stability of the network; whereas, such site changes in the smaller VLBI networks could affect their stability more. An additional consideration is that the GNSS and VLBI observing modes are different. GNSS measures the signal delay between a satellite and a receiver; whereas, VLBI measures baseline delays. The number of baselines is N(N-1)/2 for a network of N sites which as a function of N implies a quadratic increase in the number of observations compared to a linear increase for GNSS. Competing factors are 1) GNSS observation rates are significantly higher and 2) the number of VLBI observations decreases with baseline length.

Fig. 10 shows the evolution of this precision over the period 2002–2020. Each point on the curves plotted corresponds to the WRMS difference in the same 1-year window used to generate the smoothed curves in Fig. 9. The WRMS at each epoch was computed about the average difference in the one-year window of the epoch. Although the precision does have variability at a yearly scale, the trend in precision is generally decreasing such that polar motion precision for both the R1 and R4 series improved from 2002.0 to 2018.0. From 2002 to 2018, the R1 X-pole and Y-pole precisions improved by a factor of about 2.4. R4

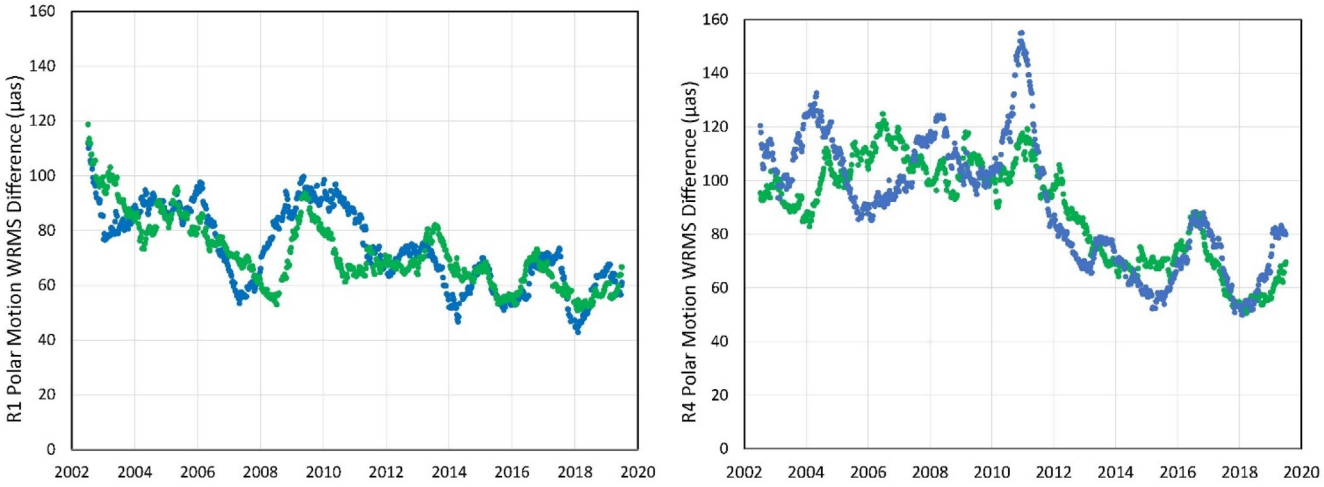

Fig. 10. WRMS of the IGS polar motion differences shown in Fig. 9 with respect to the R1 series (left plot) and the R4 series (right plot). Each point is computed for a one-year window about the corresponding epoch. The WRMS differences were computed at each epoch with respect to the mean difference in each window in Fig. 9. X-pole WRMS is plotted in blue and Y-pole WRMS in green.

X-pole and Y-pole precision improved by factors of about 2.4 and 1.9. After 2018.0, R1 and R4 precisions have become worse. This can also be seen from the formal uncertainties in Fg. 6. It appears to be largely caused by a reduction in the number of observations made and fewer stations on average in the networks.

Some of the systematic features in these plots are correlated with stations in the networks. The Fortaleza station did not observe in the R4 network from 2010.0 to 2011.5. This is correlated with the increase in X-pole precision during this time period. The peak at 2017.0 took place when the Ht15 station did not observe. Possibly the increase after 2018.5 is due to Hobart12 leaving the network. The increases seen for both R1 polar motion components around 2010 could be due Hartrao and Fortaleza not observing. Fortaleza started to observe in the R1 sessions at 2010.0 that is coincident with both components decreasing.

Since 2015, the R1 session data rate has alternated between 256 Mbps (112 odd numbered sessions) and 512 Mbps (111 even numbered sessions). The average EOP uncertainties of the 256 Mbps sessions were less than 1% better than the average of the 512 Mbps sessions. Comparing EOP with GNSS estimates from the IGS Finals series, Table 4 shows that the WRMS agreement is better for the higher data rate sessions except for Y-pole, where the 256 Mbps sessions had significantly better agreement. It is not clear why this occurs since the measurement noise associated with the 512 Mbps sessions is less by a factor of $\sqrt{2}$.

Table 4
WRMS agreements of R1 session polar motion and LOD relative to GNSS EOP from 2015 through 2019.

Parameter	256 Mbps		512 Mbps	
	WRMS	χ^2	WRMS	χ^2
X-pole (μas)	69.0	3.4	64.8	3.3
Y-pole (μas)	58.1	3.3	71.3	5.3
X-pole rate (μas/d)	152.1	2.8	137.9	2.9
Y-pole rate (μas/d)	193.0	3.9	180.5	3.7
LOD (μs/d)	15.1	7.1	13.9	6.5

5. Summary and conclusions

The EOP precision improved for both the R1 and R4 sessions from 2002.0 until 2017–2018. At this point the number of stations in the networks declined resulting in fewer observations and larger uncertainties. R1 polar motion component formal uncertainties improved by factors of 3 and 2, respectively. In terms of observed polar motion, comparisons between VLBI and GNSS EOP showed that the precision of polar motion improved by about a factor of 2.4; whereas, R4 X and Y polar motion precision improved by factors of 2.4 and 1.9, respectively. R1 UT1 formal uncertainties improved by a factor of 1.2. Although R4 formal uncertainties were significantly worse in the earlier years, they reached the same level as R1 formal uncertainties by 2017–2018. R4 polar motion formal uncertainties improved by factors of 3.5 and 2.4 and UT1 by a factor 1.6. Both the R1 and R4 networks have grown in both number of stations and the global extent of the networks, especially in the Southern Hemisphere. The number of stations has increased from 6 stations in 2002 to as many as 14 stations. The growth of the networks is the dominant effect leading to the improvement of EOP precision. The improvement was driven by the increase in the number of session observations, which increased as the number of stations in networks increased. Changes in data rate or changes in the number of sources observed in a session were less significant factors in this improvement.

The observation success rates for both R1s and R4s are about 80% consistently over the twenty years of observing.

Since each observation corresponds to a baseline, an average station success rate of about 90% is roughly consistent with an 80% observation success rate. Certainly, we need to investigate how to improve this success rate. Clearly the formal uncertainties of estimated EOP will be improved with more successful observations.

The Continuous Observing Campaign (CONT) sessions have significantly better EOP precision than the operational R1 and R4 sessions. The CONT11, CONT14, and CONT17 (Legacy-1 network) had X and Y polar motion precisions (determined by the WRMS of VLBI – GNSS differences) ranging from 19 to 27 μas and 26–29 μas, respectively (MacMillan, 2022). Based on the precisions in Fig. 10, the best R1 and R4 X/Y polar motion precision is 45/50 μas and 50/54 μas, respectively. The superior precision of the CONT sessions is likely due to using both a larger network and running the same network over the typical 15-day CONT campaign period. To try to reproduce this, the IVS ran a test in 2020–21 in which half of the annual R1 sessions were scheduled with larger networks, like the CONT networks, and observed with the 512 Mbps data rate. Preliminary analysis of sessions in the first year of the test show that agreement of polar motion estimates with GNSS is better but not as good as for CONT sessions. It is possible that there are systematic or seasonal errors that affect this series of R1s that do not contribute significantly to short-term 15-day CONT series. Practically speaking, it is not possible to run all R1 sessions with large networks as was done in this test, because stations are simply not available to do it.

In the future there will be more mixed-mode observing, which will increase the network size by adding VGOS stations to the R1 and R4 sessions. On the other hand, it is likely that some of the larger S/X antennas will stop operating as more VGOS antennas begin operating. Unattended observing will also increase the network size of the R1 and R4 sessions by allowing more stations to participate because the cost associated with observing will decrease when human operators do not need to be present for each session. It is expected that eventually the R1 and R4 series will end. However, this would require that the VGOS network does become sufficiently robust and that will probably not happen for several years.

Declaration of Competing Interest

The authors declare that they have no known competing financial interests or personal relationships that could have appeared to influence the work reported in this paper.

Acknowledgements

This work was funded under NASA Goddard Space Flight Center (United States) contract NNG17HS00C. We thank the IVS for providing the VLBI data (Nothnagel et al. 2017) that we analyzed in this paper as well as Paul Rebischung (IGN) for his reprocessed GNSS series computed with reference frame IGSR3.

Appendix A. R1 and R4 network evolution

Year	R1 Network	R4 Network
2002	Six-station network. Tigo joined the network in May 2002.	Core network of four stations but no more than six stations participated in each session.
2003	The network increased to seven stations. Hobart-26 m was added to the network in May 2003 after it was upgraded to Mark 5.	The network increased to seven stations. Seshan stopped participating but Tigo, Svetloe, and Onsala were added to the network.
2004	Matera was scheduled as a core station but went down at the beginning of the year due to rail problems. Fairbanks and Tsukuba were the only stations recording on tape by the end of the year.	Medicina was added to the network.
2005	Westford did not participate due to budgetary constraints after September 7. Matera joined the network in July after being down for 1.5 years. Fortaleza participated in two sessions after getting their Mark 5 system. Fairbanks stopped operations at the end of the year.	Matera and Zelenchukskaya joined the network, increasing the number to eight stations for some sessions. Fairbanks stopped operations at the end of the year.
2006	Fortaleza participated in several R1 sessions using 4 MHz bandwidth while the other stations used 8 MHz bandwidth. Seshan participated with only eight BBCs. Both Ny Alesund and Zelenchukskaya were tagged along to sessions in which those stations participated.	No significant change.

(*continued*)

Year	R1 Network	R4 Network
2007	Ny Alesund and Zelenchukskaya continued to be tagged along to all sessions in which the two stations participated. Seshan continued to participate in the sessions with only eight BBCs but Fortaleza started using 8 MHz bandwidth in late October (R1300).	The network lost the use of Algonquin Park and Onsala but gained the use of Badary and Westford.
2008	No significant change.	No significant change.
2009	The network was more stable with seven stations. Ny Alesund, Westford, Tigo, Hobart, Kokee, Tsukuba, Wettzell participating in at least half of the scheduled sessions. Ny Alesund was scheduled as a regular station and both Badary and Zelenchukskaya were tagged along to 13 sessions.	Westford did not participate in the network but Yebes was added. Fortaleza went down in October due to problems with the antenna azimuth bearing.
2010	Seventeen different stations participated but only seven stations participated in at least 26 of the sessions. The size of the network increased to nine stations for some of the sessions. HartRAO-26 m started participating in the network in mid-August after being down for almost two years. In addition, the new Hobart-12 m was tagged along to several sessions.	Hobart-26 m and Hobart-12 m participated in several Rapid sessions together starting in 2010.
2011	The number of participating stations increased to 21 different stations due to the addition of Katherine, Kashima-11 m, Warkworth, and Yarragadee. The size of the network for some sessions increased to 11 stations.	Fortaleza successfully returned to the network during mid-May. Starting in June, Katherine and Yarragadee participated in 11 of the sessions.
2012	The number of different stations participating in the sessions decreased because Badary, Svetloe, Kashima-11 m, and Zelechukskaya no longer participated. Some of the sessions still had 11-station networks. Urumqi was tagged along to one session in preparation to join the Rapid sessions during 2013	Tsukuba was added to the various R4 networks.
2013	The network size increased to 12 for some of the sessions and Aira participated in some sessions for the first time.	The network size increased to 12 for some of the sessions. There were 15 different stations participating in the network.
2014	Some of the R1 sessions were scheduled with 13 station networks with 20 different stations participating overall in the R1 sessions. Sejong and Tianma65 were new to the sessions.	Warkworth was added to the network during the second half of the year.
2015	Yebes-13.2 m (RAEGYEB) was tagged along to half of the remaining sessions starting April. Ishioka was tagged along to all sessions starting in October. Westford transitioned to a VGOS station and did not participate in any S/X sessions. Sessions were observed with two different frequency sequences: 256 Mbps for the odd sessions and 512 Mbps for the even sessions.	Wettzell-North was tagged along to either an R1 or R4 session each week starting in June alternating between the R1 and R4 sessions.
2016	HartRAO-15 m down from February through mid-October because of gearbox problems and did not participate in the R sessions.	Yebes-13.2 m only participated in one R4 session and did not participate in any R sessions for the remainder of the year.
2017	Hobart-12 m transitioned to a VGOS station and did not participate in any S/X sessions after late June.	Same as R1.
2018	AGGO participated in some R sessions.	Same as R1.
2019	This was the last year to distinguish between frequency sequences based on session number.	Katherine transitioned to a VGOS station and did not participate in any S/X sessions after late August.

References

Altamimi, Z., Rebischung, P., Metivier, L., Collilieux, X., 2016. ITRF2014: a new release of the international terrestrial reference frame. J. Geophys. Res. Solid Earth 121, 6109–6131. https://doi.org/10.1002/2016JB013098.

Anderson, J.M., Xu, M.H., 2018. Source structure and measurement noise are as important as all other residual sources in geodetic VLBI combined. J. Geophys. Res.: Solid Earth 123, 10–162. https://doi.org/10.1029/2018JB015550.

Berube, M., Searle, A., 2006. Algonquin Radio Observatory 2006 Annual Report. In: Behrend, D., Baver, K.D. (Eds.) IVS 2006 Annual Report NASA/TP-2007-214151.

Böhm, J., Schuh, H., 2004. Vienna mapping functions in VLBI analysis. Geophys. Res. Lett. 31. https://doi.org/10.1029/2003GL018984 L01603.

Dow, J.M., Neilan, R.E., Rizos, C., 2009. The international GNSS service in a changing landscape of global navigation satellite systems. J. Geod. 83, 1919–11198. https://doi.org/10.1007/s00190-008-0300-3.

Fey, A., Gordon, D., Jacobs, C.S., et al., 2015. The second realization of the international celestial reference frame by very long baseline interferometry. Astron. J. 150 (2), 58. https://doi.org/10.1088/0004-6256/150/58.

Gipson, J., Le Bail, K., Ma, C., 2014. The NASA Goddard Group's Source Monitoring Database and Program. In: D. Behrend, K. D. Baver, K. L. Armstrong (Eds.) IVS 2014 General Meeting Proceedings, Science Press (Beijing), pp. 390-394, ISBN 978-7-03-042974-2.

Gipson, J., 1998. Baseline Geometry and EOP, unpublished GSFC internal memo.

Gipson, J., 2010. An Introduction to Sked. In: D. Behrend, K. D. Baver (Eds.) IVS 2010 General Meeting Proceedings, pp. 77-84, NASA/CP-2010-215864.

Gipson, J. (Ed.), 2012. Sked: VLBI Scheduling Software. Program Reference Manual, Goddard Space Flight Center.

Gipson, J., 2019. How do we plan observations? – Scheduling, at VLBI school 2019. In: 3rd IVS Training School on VLBI for Geodesy and Astrometry, 14-16 March, Las Palmas, Gran Canaria. Available on vimeo: https://vimeo.com/515497131

Kingham, K., Carter, M.S., 2002, U.S. Naval Observatory Operation Center / NEOS Operation Center at USNO, In: Vandenberg, N., Baver, K.D. (Eds.), IVS 2002 Annual Report NASA/TP-2003-211619.

Klopotek, G., Hobiger, T., Haas, R., 2018. Geodetic VLBI with an artificial radio source on the Moon: a simulation study. J. Geod. 92, 457–459.

Lambert, S., Gontier, A.M., 2006. A Comparison of R1 and R4 IVS Networks. In: Behrend, D., Baver, K.D. (eds.), IVS 2006 Annual Report NASA/CP-2006-214140.

Lovell, J., et al., 2014, AuScope VLBI Project and Hobart 26-m Antennas. In: Baver, K, Behrend, D., Armstrong, K. (eds.), IVS 2014 Annual Report NASA/TP-2015-217532.

Ma, C., Sauber, J.M., Bell, L.J., Clark, T.A., Gordon, D., Himwich, W.E., Ryan, J.W., 1990. Measurement of horizontal motions in Alaska using very long baseline interferometry. J. Geophys. Res. 91, 819–829.

MacMillan, D.S., 2017. EOP and scale from continuous VLBI observing: CONT campaigns to future VGOS networks. J. Geod. 91, 819–829. https://doi.org/10.1007/s00190-017-1003-4.

MacMillan, D.S., 2022. Comparison of EOP and scale parameters estimated from the three simultaneous CONT17 VLBI observing networks. J. Geod. 96, art. 25. https://doi.org/10.1007/s00190-022-01611-2.

MacMillan, D., Cohen, S., 2004. Postseismic transient after the 2002 Denali fault earthquake from VLBI measurements at Fairbanks. In: Vandenberg, N., Baver, K.D. (Eds.), Proc. IVS 2004 General Meeting.

MacMillan, D.S., Ma, C., 2007. Radio source instability in VLBI analysis. J. Geod. 81, 443–453.

Malkin, Z., 2009. On comparison of the Earth orientation parameters obtained from different VLBI networks and observing programs. J. Geod. 83, 547–556. https://doi.org/10.1007/s00190-008-0265-2.

Niell, A., Barrett, J., Burns, A., Capallo, R., Corey, B., Derome, M., et al., 2018. Demonstration for a broadband very long baseline interferometer system: A new instrument for high-precision space geodesy. Radio Sci 53, 1269–1291.

Nothnagel, A., Artz, T., Behrend, D., Malkin, Z., 2017. International VLBI Service for Geodesy and Astrometry – Delivering high-quality products and embarking on observations of the next generation. J. Geod. 91, 711–721.

Petit, G., Luzum, B. (Eds.), 2010. IERS Conventions (2010). IERS Technical Note 36. Verlag des Bundesamts fur Kartographie und Geodasie, Franfurt am Main, Germany.

Plank, L., Lovell, J.E.J., Shabala, S., Boehm, J., Titov, O., 2015. Challenges for geodetic VLBI in the southern hemisphere. Adv. Space Res. 56, 304–313.

Ryan, J.W., Ma, C., 1998. NASA-GSFC's geodetic VLBI program: a twenty-year retrospective. Phys. Chem. Earth 23 (9–10), 1041–1052 (PII S0079–1946(98)00144-X).

Schlüter, W., Vandenberg, N.R., 2003, Geodetic VLBI – Wishes and Limitations, New Technologies in VLBI ASP Conference Series, Vol. 306, 2003 Y.C, Minh.

Schlüter, W., Behrend, D., 2007. The International VLBI Service for Geodesy and Astrometry (IVS): current capabilities and future prospects. J. Geod. 81 (379–387). https://doi.org/10.1007/s00190-006-0131-z.

Schuh, H., Charlot, P., Hase, H., et al., 2002, IVS Working Group 2 for Product Specification and Observing Programs, Final Report.

Thomas, C., MacMillan, D., 2003. CORE Operation Center Report. In: Vandenberg, N., Baver, K.D. (Eds.), IVS 2002 Annual Report NASA/TP-2003-211619.

Thomas, C., MacMillan, D., 2020. CORE Operation Center 2017-2018 Biennial Report. In: Armstrong, Baver, K.D., Behrend (Eds.) IVS 2017+2018 Biennial Report NASA/TP-2020-219041.

Titov, O., Tregoning, P., 2005. Effect of post-seismic deformation on earth orientation parameter estimates from VLBI observations: a case study at Gilcreek. Alaska. J. Geod. 79, 196–202. https://doi.org/10.1007/s00190-005-0459-9.

Vandenberg, N.R., Whitney, A.R., 2003. IVS Mark 5 Deployment Plan. http://ivscc.gsfc.nasa.gov/program/Mk5plan.pdf.

Whitney, A.R., 2005. Mark IIIA/IV/VLBA Tape formats, recording modes and compatibility revision 1.21, MIT Haystack Observatory, 10 June 2005.

Xu, M.H., Lunz, S., Anderson, J.M., Savolainen, T., Zubko, N., Schuh, H., 2021. Evidence of the Gaia–VLBI position differences being related to radio source structure. Astronomy Astrophys 647. https://doi.org/10.1051/0004-6361/202040168 A189.